A Compact Tri-band Miniaturized Antenna with Parasitic Elements Loading

Yan Deng, Xue-Fei Li, and Jing-Song Hong

Institute of Applied Physics
University of Electronic Science and Technology of China, 610054 Chengdu, China
dengyanabc@gmail.com, 13668740942@163.com, cemlab@uestc.edu.cn

Abstract ─ A compact tri-band miniaturized antenna with parasitic element loading is proposed for small form factor devices. Firstly, the dual-band antenna is proposed. Based on the theory of characteristic mode (TCM), the resonant of the metal loop decreases by adding three identical square monopole on the other side of the substrate. By exciting one of three square monopoles, the other two monopole treating as parasitic units, can lower the Q factor of the monopole and enhance the bandwidth of the antenna. Then, the tri-band antenna is proposed. By adding metal patches on the side of the parasitic elements, the higher order of the metal loop is excited and the new resonant point is created. With the adoption of the TCM, two degenerate modes are separated by adding metal strips on the metal loop to enhance the bandwidth of the low band. Also, the same way is carried out to decrease the electric size of the antenna and the size of the proposed structure meets the requirement of the electric small antenna. To verify the performance, the proposed antenna is fabricated and tested. The measured results are in agreement with simulated results.

Index Terms ─ Bandwidth enhancement, electrically small antenna (ESAs), miniaturized size, tri-band.

I. INTRODUCTION

In our daily life, many wireless devices have been successfully deployed in a wireless communication system such as laptops, Global Positioning System, Bluetooth. Recently, many researchers attach more attention to the electric small antenna for a huge demand for the small form factor devices applied in the smart city.

A widely recognized fact is that the electric small antenna possesses the characteristic of $k \cdot a < 1$. Many technologies have been developed to decrease the size of the antenna. Grounding on the analysis and calculation of CRLH LT theory [1], the antenna designed based on CRLH metamaterial possesses the characteristic of electric small size. Folded patch [2-4], defected ground plane [5-7], and virtually shorting pin [8,9] are three techniques to decrease the size of the antenna. By combining three approaches, the antenna in [8] achieves size reduction more than 80% compared to the conventional half-wave patch antenna. Moreover, the employed of a high permittivity substrate to miniaturize the size of antenna report in [10] and a size reduction more than 80% is achieved.

Also, the multi-band antenna is required to satisfy the requirement of the equipment in different applications. Till now, the variously printed antenna has manufactured for the multi-band application. In paper [11-13], the different shapes of metal were printed on the front and back sides of the substrate to produce diverse resonance. The diode serving as a configuration structure makes the antenna resonance in the upper and low band [14]. With high and low voltage, the resonant frequency of the antenna is varied to generate different resonant modes. In terms of Babinet theory, slot [15] is treated as the dipole. Therefore, the same way is carried out in the slot antenna to generate multi-band.

Although many methods have been adopted in multi-band miniaturized antenna, there still exist some problems. In [16-19], various complex printed shapes were employed to achieve multi-band characteristics. With those shapes utilized, it's difficult to design and optimize the antenna. In [20], the dual-band patch antenna achieves a 74% miniaturized ratio at 2.4 GHz, but the -6 dB impedance bandwidth of the antenna is 40 MHz at the 2.4 GHz and 1.5 GHz at 5.2 GHz.

In this paper, a compact tri-band miniaturized antenna is proposed to reduce the electric size and enhance the bandwidth of the antenna. With the TCM adopted, it's easy and accurate to design and optimize the antenna. With three square monopoles adding, the resonant point of the antenna in the low band decrease, and the bandwidth of the antenna in the high band increase. In addition, two metal patches add on the side of the parasitic elements to generate the high order mode of the metal loop. Finally, the performance of the antenna in each band can be efficiently controlled by adding strips on the metal loop. The proposed antenna possesses with simple structure meeting the requirement of the WLAN/WiMAX application.

Submitted On: April 2, 2020
Accepted On: May 16, 2020

II. ANTENNA DESIGN

A. Antenna geometry and evolution steps

Figure 1 is the drawing of the proposed antenna (26.4×26.4×1mm^3). The dielectric serving as the substrate of the antenna is FR-4. The height of substrate and copper are 1mm and 0.018mm respectively. Figure 2 depicts the four steps to designing the proposed compact tri-band miniaturized antenna. The curves presenting in Fig. 3 (b) are the reflection coefficient of the antenna with a different structure. The label of curves in Fig. 3 (b) corresponds to the label in Fig. 2. To explore the working principle of the proposed antenna, the characteristic mode analysis (CMA) use here to analyze the performance of the antenna with the adoption of CST MICROWAVE STUDIO.

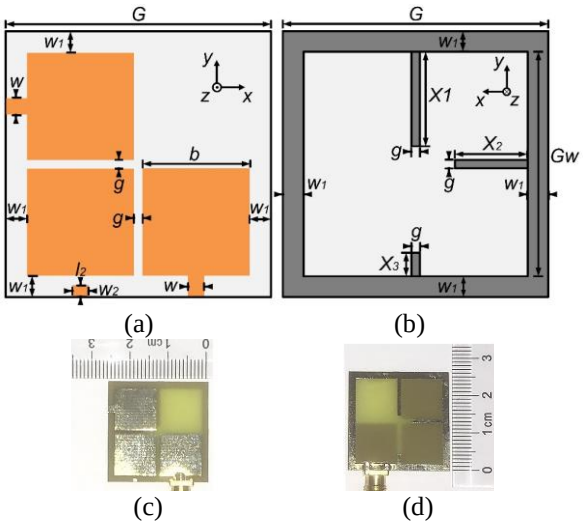

Fig. 1. Topology of the proposed antenna: (a) top view, (b) bottom view, (c) top view of the fabricated antenna, and (d) bottom view of the fabricated antenna.

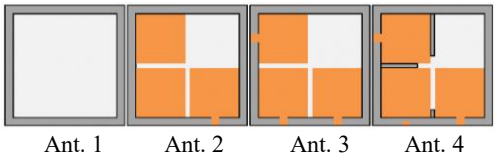

Fig. 2. Four steps to design the proposed antenna.

B. Theory of characteristic mode

Basing on the method of moment (MOM) which is the mathematical concept, a unified matrix approach treating for field problems is given in [21]. And, the theory and the computation of CMs for conducting bodies are given in [22] and [23]. Then, TCM applied in a dielectric and magnetic material is given in [24].

To summary, the TCM gives three important indices λ_n , α_n and Modal significance (MS) to judge the performance of the characteristic mode.

λ_n called eigenvalue represent the degree of resonant at *n*th modes. The value of λ_n is calculated by equation: $X(J_N) = \lambda_N R(J_N)$, where $X(J_N)$ and $R(J_N)$ are the imaginary and real parts of the impedance at the corresponding mode in matrix *Z*. The corresponded mode is likely to resonate when λ_n approaches zero.

α_n called the weighting coefficient obtain from the equation: $J = \sum \alpha_N J_N$, where *J* is current on conducting bodies when an electric field impress and J_N is a series of complete orthogonality eigenfunctions.

The resonant frequency and the resonant degree of characteristic mode can also be judged from the value of MS. The value of MS is calculated by the equation: $MS = |1/(1 + j\alpha_N)|$. The corresponded mode is likely to resonate when MS approaches one.

C. The mechanism of Ant. 1

The loop antenna widely applies to the wireless communication system. Here, we put a loop on the surface of the substrate.

The value of *Gl* is determined by:

$$Gl \approx \frac{c}{4\times f_0}, \tag{1}$$

where c is the speed at which light travels in a vacuum, f_0 is the frequency where the eigenvalues of the Ant.1 equal to zero. The value of *Gl* is related to the value of *G* and *Gw* giving by:

$$Gl = \frac{G+Gw}{2}. \tag{2}$$

Figure 3 (a) shows the eigenvalues of the proposed structure Ant. 1 with the adaptation of TCM. We can notice that the curves of the two eigenvalues coincide with each other and the value of eigenvalues equal to zero at 3.1 GHz. Therefore, the metal loop possesses two degenerate modes at 3.1 GHz.

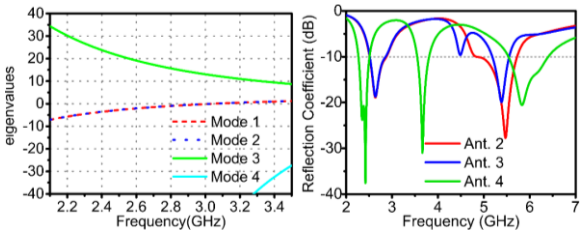

Fig. 3. The curve of the antenna: (a) eigenvalues of the metal loop, and (b) reflection coefficient of antennas.

D. The mechanism of Ant. 2

By adding three square metal patches in Ant. 1, the electrical size of the antenna decreases, and the bandwidth of the antenna in the upper band increases. The size of the square metal patch is determined by:

$$b \approx \frac{3 \times c}{8 \times f_1 \times \sqrt{\varepsilon_{rd}}}, \quad (3)$$

where f_1 is the resonant frequency of the Ant. 2 in the upper band.

As showing in Fig. 4 (a), with three monopoles loading, the point where eigenvalues equal to zero, varies from 3.1 GHz to 2.7 GHz in the low band. When three monopoles loading on the surface of the substrate, it can change the impedance characteristic of the metal loop leading to the resonant point decrease.

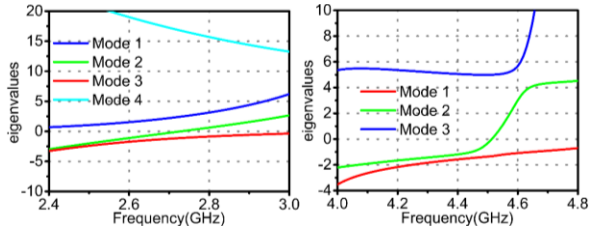

Fig. 4. Eigenvalues of the antenna: (a) Ant. 2 in the low band, and (b) Ant. 3 in the middle band.

Fig. 5. Simulated eigencurrent distribution of Ant. 2 at 2.7 GHz: (a) Mode 1, (b) Mode 2, and (c) Mode 3.

To enhance the impedance bandwidth in the upper band, the parasitic loading technique studying in paper [25] use here. By exciting one of three square metal patches, the other two metal patches treating as parasitic units, can lower the Q factor of the monopole and enhance the bandwidth of the antenna in the upper band.

The -10dB impedance bandwidth of Ant. 2 covering the frequency of 2.52 GHz-2.87 GHz (WiMAX band) and 4.84 GHz-5.72 GHz (WLAN band) is shown in Fig. 3 (Ant. 2). Moreover, the antenna possesses with omnidirectional radiation pattern in the low band. For the upper band, the antenna is provided with a 4.09 dBi peak gain at 5.5 GHz.

E. The mechanism of Ant. 3

In the process of CMA [26], the shorting pin and capacitance are traditional ways to modulate the performance of the antenna. Here, we add the patches on the side of the parasitic metal patches to vary the performance of the Ant. 2. In comparison with the curve of Ant. 2 in Fig. 3 (b), the curve of Ant. 3 changes greatly in the middle and up band, while the curve of Ant. 3 remains the same in the low band.

For the low band, the current distribution of the characteristic mode presents in Fig. 5. Few currents distribute on the right side of the PEC where two metal patches are added. Therefore, the metal patches have less influence on the current distribution of Mode 2, and the performance of the antenna remains unchanged.

For the upper band, the antenna work in monopole mode. The metal patches adding to the side of the monopole influence the impedance of two parasitic radiators. Therefore, the impedance matching of the antenna becomes worse and the impedance bandwidth of the antenna becomes narrow in the upper band.

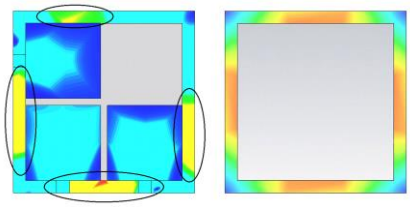

Fig. 6. Simulated eigencurrent distribution: (a) Mode 2 of Ant. 3 at 4.5 GHz, and (b) Mode 4 of Ant. 1.

In the middle band, the CMA uses here to figure out the new mode. Judging from the eigenvalues in Fig. 4 (b), we can conclude that Mode 2 contributes to the antenna resonant in the middle band. Furthermore, the eigencurrent of the metal loop's high-order is given to prove that Mode 2 is the high-order mode of the metal loop. As we can see from Figs. 6 (a) and (b), the primary current distribution of two modes is similar by contrasting the maximum current in each arm. However, the current distribution is unbalanced in each arm of the Mode 2 showing in Fig. 6 (a). And, the monopole and metal patches loading are the main reasons leading to the unbalanced distribution of the current.

F. The mechanism of Ant. 4

The curve of the reflection coefficient in Fig. 3 (b) illustrates that the Ant. 3 is a tri-band antenna and possesses narrow bandwidth in the upper band. Therefore, we can take some measures to improve the impedance bandwidth in the upper band. The strips adding on the metal loop is shown in Fig. 2 (Ant. 4) for changing the impedance of monopole. With the adaptation of CAM, we figure out the function of strips adding in the different places separately.

In the low band, Mode 2 and Mode 3 contribute to the resonance of the antenna according to the eigenvalues in Fig. 4. As we can see from Fig. 5, the strip X_1 and X_3 add to the maximum current distribution of Mode 2 and the minimum current distribution of Mode 3 while the strip X_2 adds to the minimum current

distribution of Mode 2 and the maximum current distribution of Mode 3. With the strip adding to the minimum of current distribution, the impedance of the metal loop changes leading to the mode resonant point shifts to low frequency.

Therefore, the performance of Mode 2 has a relation to the strip X_2. Also, the performance of Mode 3 has a relation to the strip X_1 and X_3. To verify this point of the view, the strips X_1, X_2 and X_3 add separately in Ant. 3. And the reflection coefficient and modal significance of Ant. 3 with strips X_1, X_2 and X_3 adding separately shows in Fig. 7.

The strip X_1 with the length of 10mm adds in Ant. 3. In Fig. 7 (b), the frequency of Mode 3 shifts to low band equal to 2.34 GHz which corresponded to the resonant point showing in the red line of Fig. 7 (a). Moreover, the frequency of Mode 2 shifts lightly.

Add a strip X_2 with a length of 8mm to Ant. 3. In Fig. 7 (c), the frequency of Mode 2 shifts to low band equal to 2.42 GHz which corresponded to the resonant point showing in the blue line of Fig. 7 (a). Furthermore, the frequency of Mode 3 shifts lightly.

Owing to the length of the X_3 is short so that the resonant point of Mode 2 and Mode 3 shift lightly.

And the middle band of the antenna is the high order mode of the metal loop. Therefore, the resonant frequency shifts as the low band.

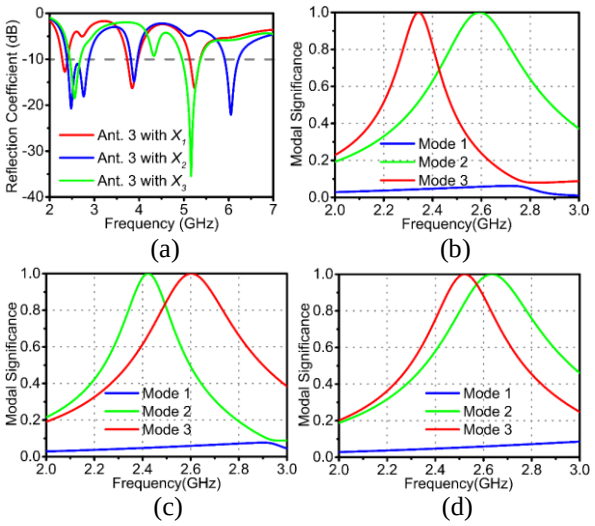

Fig. 7. The simulated results of Ant. 3 with strip loading separately: (a) reflection coefficient, (b) modal significance with X_1 loading, (c) modal significance with X_2 loading, and (d) Modal significance with X_3 loading.

G. Parametric study

Parametric studies are carried to improve the performance of Ant. 3 with the strips X_1, X_2 and X_3 loading.

In Fig. 8, two degenerate modes in the low band coincide with the increasing of X_2 and separate with the increasing of X_1 and X_3. Therefore, the changes in Fig. 8 are consistent with the changes in Fig. 7.

As we can see from Fig. 8 (a), two resonant points shift to the low frequency and become closer with increasing the length of X_1 in the upper band. Furthermore, with increasing of X_2, the first resonant point in the upper band still unchanged and the second resonant point in the upper band shifts to the low band showing in Fig. 8 (b). According to Fig. 8 (c), the performance of the antenna in the upper band is better with the shorter length of X_3.

In Fig. 8 (d), the performance of the Ant. 4 in the upper band is getting better with the value of the w_2 and l_2 changing.

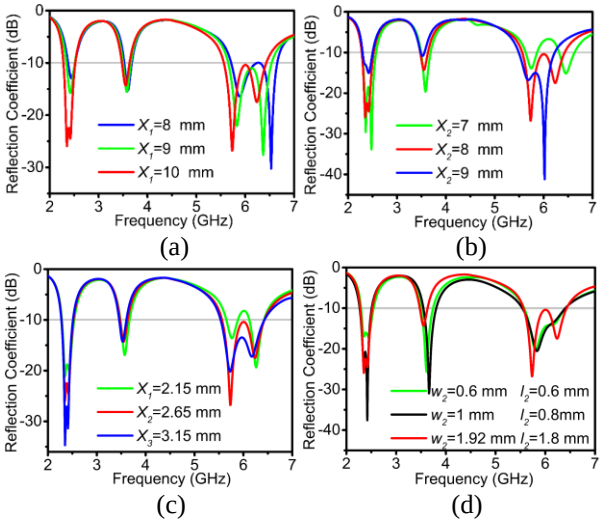

Fig. 8. Reflection coefficient of Ant. 4 with different parameters' value: (a) X_1; (b) X_2; (c) X_3; (d) w_2 and l_2.

Table 1: The optimized parameters of the Ant. 4

Parameter	Value (mm)	Parameter	Value (mm)
G	26.4	b	10.9
Gw	22.8	h	1
g	1	l_2	0.8
w	1.92	X_1	10
w_1	1.8	X_2	8
w_2	1	X_3	2.65

III. MEASURED RESULTS

The optimized parameters are given in Table 1. And, to confirm the validity of the design, the proposed Ant. 4 is fabricated and measured as shown in Fig. 9.

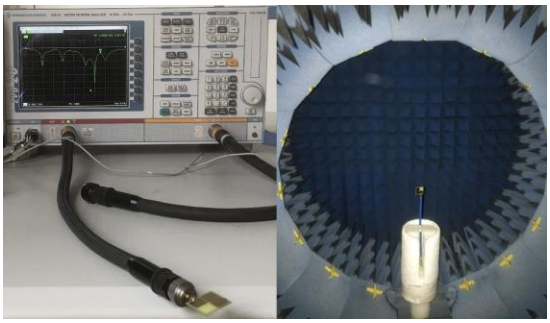

Fig. 9. Measured environment.

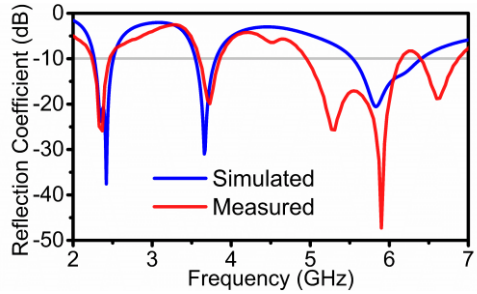

Fig. 10. The measured and simulated S_{11}.

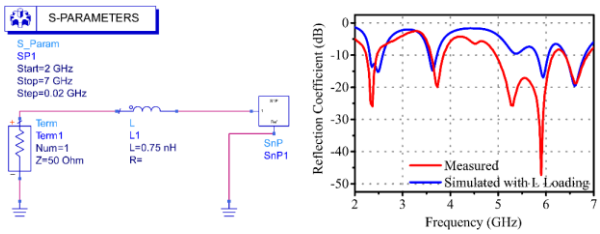

(a) (b)

Fig. 11. The influence of the inductor on the reflection coefficient of the antenna: (a) Simulated model considering the SMA, and (b) The results of the measured and simulated reflection coefficient.

A. S-parameters

The measured and simulated value of the reflection coefficient is presented in Fig. 10. The solid red line shows the result of the measured reflection coefficient, while the solid blue line exhibits the consequence of the simulated reflection coefficient. The measured bandwidth where S_{11}<-10dB covers 2.24-2.48 GHz, 3.60-3.85 GHz, 4.94-6.15 GHz, and 6.40-6.86 GHz. The relative bandwidth of the proposed antenna is 10.2%, 6.7%, 21.8%, and 6.9%.

The difference between simulated and measured results is primarily due to the adding of feeding SMA in measurement. The soldering and the adding of the SMA introduce extra inductors leading to the reflection coefficient of antenna change greatly in the upper band. To verify it, the simulated model and result exhibits in Fig. 11. As we can see from Fig. 11 (b), the simulated result corresponds to the measured result.

B. Radiation performance

The antenna measurement system SATIMO [27] is employed to calculate the performance of the antenna. With this equipment, the 2-D electric field data, the realized peak gain and the total efficiency are calculated. In Fig. 12, the radiation pattern at frequencies of 2.37, 3.73, 5.31, 5.90 GHz are selected to represent the radiation performances of the antenna. In Fig. 12, we can come up with that the antenna can achieve omnidirectional radiation in the low and middle band. For the upper band, the antenna cannot achieve the omnidirectional radiation but still acceptable. And this phenomenon caused by the strips adding on the metal loop to enhance the impedance bandwidth.

The total efficiency and peak gain are exhibited in Fig. 13. For the low band, the measured value of peak gain is lower than the simulated gain of 0.8 dBi owing to lower efficiency.

According to [28], the total efficiency of the antenna is determined by the reflection efficiency at the input terminals of the antenna, conduction efficiency and dielectric efficiency of the antenna.

And, SATIMO [27] measures the efficiency of the antenna according to this principle. This equipment measures radiation characteristics and the reflection coefficient of the antenna. Then, it calculates radiation efficiency by the definition in [28].

The antenna is electrically small in the lower band. Therefore, the small size of the ground plane leading to the currents flows back to the outer conductor surface of the cable. According to [29], this phenomenon will cause ripples in the radiation pattern. To improve the accuracy of the measured results, the feeding cable cover with an EM suppressant material [30] to absorb the currents flowing back to the outer conductor surface by SATIMO. The radiation energy absorbed by an EM suppressant material causes a decrease in the measured gain and efficiency.

To verify this point of view, the model of the feeding cable used in the Starlab System is built-in HFSS according to [30]. The simulated and measured efficiency of the antenna in the low band shows in Fig. 13. Owing to the feeding cable effects described above, the curve of the measured efficiency is corresponding to the simulated efficiency with the employ of the cable model in the low band. Therefore, we can conclude that the feeding cable used in the Starlab System absorbs the energy leading to the decreasing of the radiation efficiency in the low band. However, this part of the energy which absorbs by an EM suppressant material is radiated by antenna according to [29] and the gain of antenna approach to the simulated value in the application.

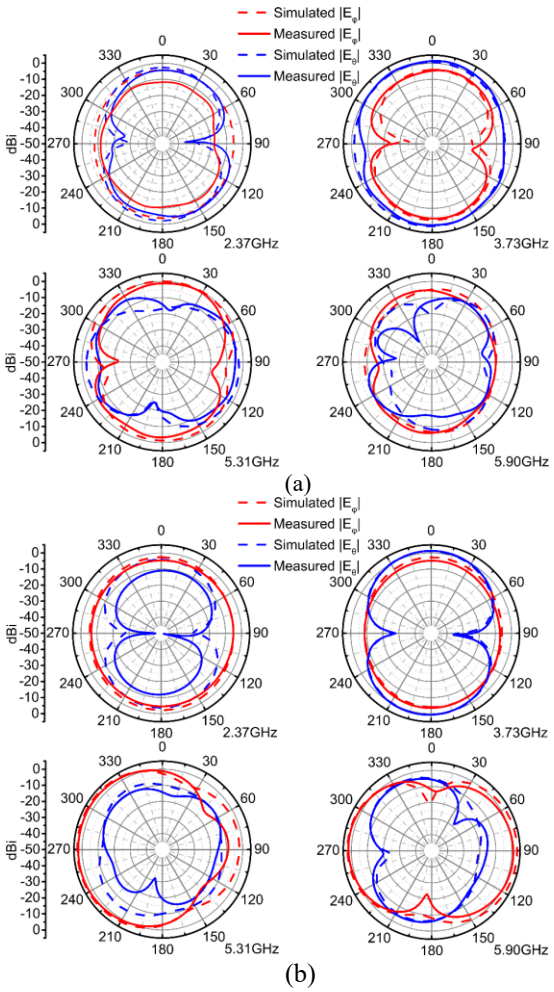

Fig. 12. The radiation pattern of the proposed antenna: (a) *xoz* plane and (b) *yoz* plane.

In Fig. 13, the curves of simulated and measured results are corresponding better. For the middle band, the measured value of peak gain lies between 2.4 and 2.9 dBi company with total efficiency vary from 69% to 75%. For the upper band, the measured value of peak gain ranges from 1.5 to 3.3 dBi with the total efficiency fluctuation between 53% and 62%.

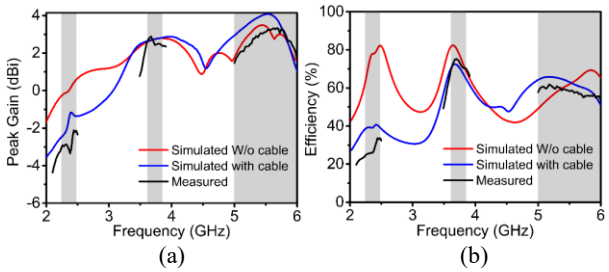

Fig. 13. The simulated and measured results of the antenna: (a) peak gain and (b) efficiency.

Table 2: Performance comparison

Reference	$k \cdot a$	First Band Bandwidth	Total Bandwidth
[9]	1.8	0.8%	3%
[16]	1.6	4.2%	12.4%
[17]	1.4	11.2%	20.4%
[31]	0.9	6%	20.7%
[32]	1.4	20.3%	32%
Proposed	0.9	10.2%	45.6%

The measurement characteristics of the proposed antenna are utilized to compare with previous works in Table 2. All of those multi-band antenna focus on the electrical small characteristic in the first band. The proposed antenna possesses the lowest value of $k \cdot a$ equal to 0.9 when we consider the first band frequency. Despite the impedance bandwidth restricted by antenna circumscribed sphere's radius, the proposed antenna achieves wider impedance bandwidth up to 10.2% in the low band with the smallest electrical size. Besides, the proposed antenna also exhibits a wider impedance bandwidth compared to the other five antennas when we consider the summation of each impedance bandwidth.

IV. CONCLUSION

A single fed novel structure with wide impedance bandwidth and miniaturized size is presented for small form factor wireless devices. The monopole serving as the radiator in the upper band is properly placed nearby the metal loop to decrease the electric size of the antenna. Moreover, the metal patches add to excite higher-order mode of metal loop leading to another resonance point achieved. To realize the better performance in each band, the metal strips are introduced to enhance bandwidth and decrease the electric size of the antenna. It is observed that by altering the performance of the monopole and metal loop, the antenna resonant in the WiMAX band and achieves better performance in the WLAN band. The prototype achieves the miniaturized structure with a size of $0.21 \times 0.21 \times 0.008$ λ3 and the 10.2% impedance bandwidth in the low band. For a middle and upper band of the antenna, the measured impedance bandwidth equal to 6.7% and 21.8% respectively.

REFERENCES

[1] A. Lai, C. Caloz, and T. Itoh, "Composite right/left-handed transmission line metamaterials," *IEEE Microw. Mag.*, vol. 5, no. 3, pp. 34-50, Sep. 2004.

[2] L. Zaid, G. Kossiavas, J. Y. Dauvignac, J. Cazajous, and A. Papiemik, "Dual-frequency and broad-band antennas with stacked quarter wavelength elements," *IEEE Trans. Antennas Propag.*, vol. 47, no. 4, pp. 654-660, Apr. 1999.

[3] C. Y. Chiu, K. M. Shum, C. H. Chan, and K. M.

Luk, "Bandwidth enhancement technique for quarter-wave patch antennas," *IEEE Antennas Wirel. Propag. Lett.*, vol. 2, pp. 130-132, 2003.

[4] S. H. Yeung, K. F. Man, K. M. Luk, and C. H. Chan, "A trapeizform U-slot folded patch feed antenna design optimized with jumping genes evolutionary algorithm," *IEEE Trans. Antennas Propag.*, vol. 56, no. 2, pp. 571-577, 2008.

[5] H. D. Chen, "Compact circularly polarised microstrip antenna with slotted ground plane," *Electron. Lett.*, vol. 38, no. 13, pp. 616-617, 2002.

[6] J. S. Kuo and G. B. Hsieh, "Gain enhancement of a circularly polarized equilateral-triangular microstrip antenna with a slotted ground plane," *IEEE Trans. Antennas Propag.*, vol. 51, no. 7, pp. 1652-1656, July 2003.

[7] D. Wang, H. Wong, and C. H. Chan, "Small circularly polarized patch antenna," *in 2011 International Workshop on Antenna Technology (iWAT)*, Hong Kong, China, pp. 271-273, 2011.

[8] H. Wong, K. K. So, K. B. Ng, K. M. Luk, C. H. Chan, and Q. Xue, "Virtually shorted patch antenna for circular polarization," *IEEE Antennas Wirel. Propag. Lett.*, vol. 9, pp. 1213-1216, 2010.

[9] A. Boukarkar, X. Q. Lin, Y. Jiang, and Y. Q. Yu, "Miniaturized single-feed multiband patch antennas," *IEEE Trans. Antennas Propag.*, vol. 65, no. 2, pp. 850-854, Feb. 2017.

[10] H. M. Chen, Y. K. Wang, Y. F. Lin, C. Y. Lin, and S. C. Pan, "Microstrip-fed circularly polarized square-ring patch antenna for GPS applications," *IEEE Trans. Antennas Propag.*, vol. 57, no. 4, pp. 1264-1267, Apr. 2009.

[11] B. Li, J. S. Hong, and B. Z. Wang, "A novel circular disc monopole antenna for dual-band WLAN applications," *Appl. Comput. Electromagn Soc. J.*, vol. 27, no. 5, pp. 441-448, May 2012.

[12] S. A. Rezaeieh and A. M. Abbosh, "Compact planar loop–dipole composite antenna with director for bandwidth enhancement and back radiation suppression," *IEEE Trans. Antennas Propag.*, vol. 64, no. 8, pp. 3723-3728, Aug. 2016.

[13] D. L. Jin, T. T. Bu, J. S. Hong, J. F. Wang, and H. Xiong, "A tri-band antenna for wireless applications using slot-type SRR," *Appl. Comput. Electromagn Soc. J.*, vol. 29, no. 1, pp. 47-53, Jan. 2014.

[14] G. M. Zhang, J. S. Hong, B. Z. Wang, and G. B. Song, "A novel frequency reconfigurable monopole antenna using PIN diode for WLAN/WIMAX applications," *Appl. Comput. Electromagn Soc. J.*, vol. 27, no. 3, pp. 256-260, Mar. 2012.

[15] C. T. Lee, S. W. Su, S. C. Chen, and C. S. Fu, "Low-cost, direct-fed slot antenna built in metal cover of notebook computer for 2.4-/5.2-/5.8-GHz WLAN operation," *IEEE Trans. Antennas Propag.*, vol. 65, no. 5, pp. 2677-2682, May 2017.

[16] M. P. Jayakrishnan, K. Vasudevan, M. Ameen, P. Mohanan, and S. Mathew, "Compact dual polarised V slit, stub and slot embedded circular patch antenna for UMTS/WiMAX/WLAN applications," *Electron. Lett.*, vol. 52, no. 17, pp. 1425-1426, Aug. 2016.

[17] S. Mathew, R. Anitha, U. Deepak, C. K. Aanandan, P. Mohanan, and K. Vasudevan, "A compact tri-band dual-polarized corner-truncated sectoral patch antenna," *IEEE Trans. Antennas Propag*., vol. 63, no. 12, pp. 5842-5845, Dec. 2015.

[18] M. C. Tang and R. W. Ziolkowski, "A study of low-profile, broadside radiation, efficient, electrically small antennas based on complementary split ring resonators," *IEEE Trans. Antennas Propag.*, vol. 61, no. 9, pp. 4419-4430, Sep. 2013.

[19] S. Verma and P. Kumar, "Printed Newton's egg curved monopole antenna for ultrawideband applications," *IET Microw. Antennas Propag.*, vol. 8, no. 4, pp. 278-286, Mar. 2014.

[20] A. A. Salih and M. S. Sharawi, "A dual-band highly miniaturized patch antenna," *IEEE Antennas Wirel. Propag. Lett.*, vol. 15, pp. 1783-1786, 2016.

[21] R. F. Harrington, "Matrix methods for field problems," *Proc. IEEE*, vol. 55, no. 2, pp. 136-149, 1967.

[22] R. Harrington and J. Mautz, "Theory of characteristic modes for conducting bodies," *IEEE Trans. Antennas Propag.*, vol. 19, no. 5, pp. 622-628, Sep. 1971.

[23] R. Harrington and J. Mautz, "Computation of characteristic modes for conducting bodies," *IEEE Trans. Antennas Propag.*, vol. 19, no. 5, pp. 629-639, Sep. 1971.

[24] R. Harrington, J. Mautz, and Y. Chang, "Characteristic modes for dielectric and magnetic bodies," *IEEE Trans. Antennas Propag.*, vol. 20, no. 2, pp. 194-198, Mar. 1972.

[25] C. Wood, "Improved bandwidth of microstrip antennas using parasitic elements," *IEE Proc. H Microw. Opt. Antennas UK*, vol. 127, no. 4, pp. 231-234, 1980.

[26] C. Deng, Z. Feng, and S. V. Hum, "MIMO mobile handset antenna merging characteristic modes for increased bandwidth," *IEEE Trans. Antennas Propagat.*, vol. 64, no. 7, pp. 2660-2667, July 2016.

[27] [Online]. Available: https://www.mvg-world.com/

[28] C. A. Balanis, *Antenna Theory–Analysis and Design*. 3rd ed. Hoboken, NJ, USA: John Wiley & Sons, 2005.

[29] L. Liu, S. W. Cheung, Y. F. Weng, and T. I. Yuk, "Cable effects on measuring small planar UWB monopole antennas," *in Ultra Wideband - Current Status and Future Trends*, M. Matin, Ed. InTech, pp. 274-294, 2012.

[30] L. Liu, Y. F. Weng, S. W. Cheung, T. I. Yuk, and L. J. Foged, "Modeling of cable for measurements of small monopole antennas," *in 2011 Loughborough Antennas & Propagation Conference*, Loughborough, United Kingdom, pp. 1-4, 2011.

[31] P. S. Bakariya, S. Dwari, M. Sarkar, and M. K. Mandal, "Proximity-coupled microstrip antenna for bluetooth, WiMAX, and WLAN applications," *IEEE Antennas Wirel. Propag. Lett.*, vol. 14, pp. 755-758, 2015.

[32] M. P. Jayakrishnan, K. Vasudevan, M. Ameen, P. Mohanan, and S. Mathew, "Compact dual polarised V slit, stub and slot embedded circular patch antenna for UMTS/WiMAX/WLAN applications," *Electron. Lett.*, vol. 52, no. 17, pp. 1425-1426, Aug. 2016.